ASME Journal of Applied Mechanics
Online journal at:
https://asmedigitalcollection.asme.org/appliedmechanics

Yijie Cai
State Key Laboratory of Fluid Power and Mechatronic Systems,
Key Laboratory of Soft Machines and Smart Devices of Zhejiang Province,
Center for X-Mechanics;
Department of Engineering Mechanics,
Zhejiang University,
Hangzhou 310027, China
e-mail: yijiecai@zju.edu.cn

Zihang Shen
State Key Laboratory of Fluid Power and Mechatronic Systems,
Key Laboratory of Soft Machines and Smart Devices of Zhejiang Province,
Center for X-Mechanics;
Department of Engineering Mechanics,
Zhejiang University,
Hangzhou 310027, China
e-mail: 12124089@zju.edu.cn

Zheng Jia[1]
State Key Laboratory of Fluid Power and Mechatronic Systems,
Key Laboratory of Soft Machines and Smart Devices of Zhejiang Province,
Center for X-Mechanics;
Department of Engineering Mechanics,
Zhejiang University,
Hangzhou 310027, China
e-mail: zheng.jia@zju.edu.cn

Fracture Toughness of Hydrogel Laminates: Experiments, Theory, and Modeling

Possessing enhanced mechanical durability and multiple novel functions, hydrogel laminates have found wide applications in diverse areas, including stretchable and bio-integrated electronics, soft robotics, tissue engineering, and biomedical devices. In the aforementioned scenarios, hydrogels are often required to sustain large deformation without mechanical failure over a long time. Compared to the fast movement in functions design, the failure mechanism of hydrogel laminates has been much less explored and researched, as well as laminates' fracture toughness—a key parameter characterizing their fracture behavior. To address this largely unexplored issue, this article further studies the fracture toughness of hydrogel laminates both experimentally and theoretically. A kind of modified pure-shear test suitable for measuring the fracture toughness of hydrogel laminates is proposed, which is then applied to testing a PAAm-PAA laminate's toughness. Through theoretical analysis and numerical modeling, the experimentally observed enhancement in the fracture toughness of PAAm-PAA laminates is explained—the fracture toughness of the laminates covers the energy required for both the crack and concomitant interfacial delamination to propagate, and the theoretical predictions agree well with the experimental results. The results from this study provide quantitative guidance for understanding the fracture behavior of hydrogel laminates. [DOI: 10.1115/1.4063144]

Keywords: hydrogel laminates, fracture toughness, interfacial delamination, toughness measurement, fracture energy

1 Introduction

Hydrogels, as soft materials composed of water-infiltrated polymer networks, possess unique chemical and mechanical characteristics similar to biological tissues and desirable electronic properties. Benefitting from these superiorities, hydrogels have set off a craze in biomedical fields serving as wound dressing [1], tissue repair [2], and cell stimulators [3], as well as in non-medical areas as ionic loudspeakers [4], artificial muscles [5], artificial skins [6], ionotronic luminescent devices [7], soft robots [8], and all solid-state supercapacitors [9]. Nevertheless, improving the mechanical durability of hydrogels has long been an important task for researchers, considering that hydrogels consist of sparse polymer networks infiltrated by a large amount of water and are naturally brittle. Notably, there exist soft materials that are mechanically robust and stable in various environments, such as elastomers and double-network gels. Since the merits of such soft materials and hydrogels are complementary to each other, it is naturally desirable to integrate them into laminate structures that can be applied in mechanically demanding environments and enable new functions.

As a matter of fact, in everyday life, there have already existed numerous natural and synthetic hydrogel laminates, which tend to bear certain mechanical loads in their application scenarios. In nature, mammalian skins laminate elastomer-like epidermis and hydrogel-like dermis into hybrids with robust interfaces (e.g., interfacial toughness over 100 J/m^2) [10] and functional microstructures (e.g., blood and lymphatic vessels). Also, in industry, as a new type of material system for environmental and health monitoring, a hydrogel interferometer based on a single hydrogel thin film covalently bonded to a reflective substrate is reported, which is designed to be a simple and universal adaptive color platform with high robustness [11]. Inspired by the deformation mechanism of Drosera leaves, a novel method for lipophilic drug release based on a dual pH-responsive hydrogel actuator is proposed, where the capsule switch is fabricated with a double-layer structure made of two kinds of pH-responsive hydrogels that can meet the specific environmental needs [12]. To harness their unique biomedical properties, in the current era of mobile health, hydrogels are also selected as ideal protective matrix/coating materials for electronics and devices to achieve long-term effective bio-integrations [13,14]. Moreover, by integrating stretchable functional electronic components such as conductors, microchips, transducers, resistors, and capacitors into tough hydrogel matrices that contain significant

[1]Corresponding author.

Contributed by the Applied Mechanics Division of ASME for publication in the Journal of Applied Mechanics. Manuscript received June 19, 2023; final manuscript received August 7, 2023; published online August 25, 2023. Assoc. Editor: Jian Wu.

amounts of water (e.g., 70–95 wt%), hydrogel-based electrical devices possessing mechanical robustness, high stretchability, and multiple novel functions are developed [4,15–17].

Yet, although it is known that forming laminate structures can help hydrogels sustain large mechanical loads without failure—which, moreover, has found wide application in mechanically demanding environments, concrete analysis about it is deficient, and the mechanisms behind it remain ill defined. Compared to the fast movement in functions design, the failure mechanics of layered hydrogel hybrids have been much less explored, where present studies of soft laminate structures' fracture behavior mainly focus on their performance of stretchability [18–23]. Very recently, Cai et al. intensively studied the superior fracture properties of hydrogel laminates distinct from homogeneous hydrogels and proposed a structure-based strategy for enhancing the fracture resistance of hydrogels by regulating the energy release rate accordingly [24]. However, in the aforementioned study, the critical stretch for crack propagation is adopted to evaluate the hydrogel laminates' fracture performance, and there is still a paucity of further research on laminates' fracture toughness—a key parameter characterizing their fracture behavior. Aiming to address this largely unexplored issue, in this article, the fracture toughness of hydrogel laminates is experimentally measured and theoretically analyzed. Here, considering that the prevailing fracture mode of soft layered materials is channel cracking in its surface layer [20], we define the fracture toughness of the hydrogel laminates as the energy required to advance a crack in the film by a unit area. The rest of this article is organized as follows. A kind of modified pure-shear test suitable for measuring the fracture toughness of hydrogel laminates is proposed, as the traditional method does not apply to hydrogel laminates. The method is then applied to test the fracture toughness of a hydrogel laminate consisting of polyacrylamide (PAAm) hydrogel and poly-(acrylic acid) (PAA) hydrogel in Sec. 2. Through theoretical analysis and numerical modeling, the experimentally observed enhancement in the fracture toughness of PAAm-PAA laminates is explained in Sec. 3. Concluding remarks are provided in Sec. 4.

2 Experimental Section

2.1 Modified Pure-Shear Test for Hydrogel Laminates. To measure the fracture toughness of homogeneous soft materials such as elastomers and gels, one generally accepted method is to conduct the classical pure-shear test [25–28]. Let us consider the case of monolayer hydrogels; as Fig. 1(*a*) illustrates, two identical hydrogel pieces are prepared using the same material, and their geometry sizes, including thickness T, width W, and height H, are also equal, where $W \gg H \gg T$. Both of them are gripped by rigid clamps, which are placed along the width direction of the specimens. A precrack whose length is ~0.5 W is introduced into the first specimen, and then it is gradually stretched along the height direction until the crack starts to propagate, with the critical

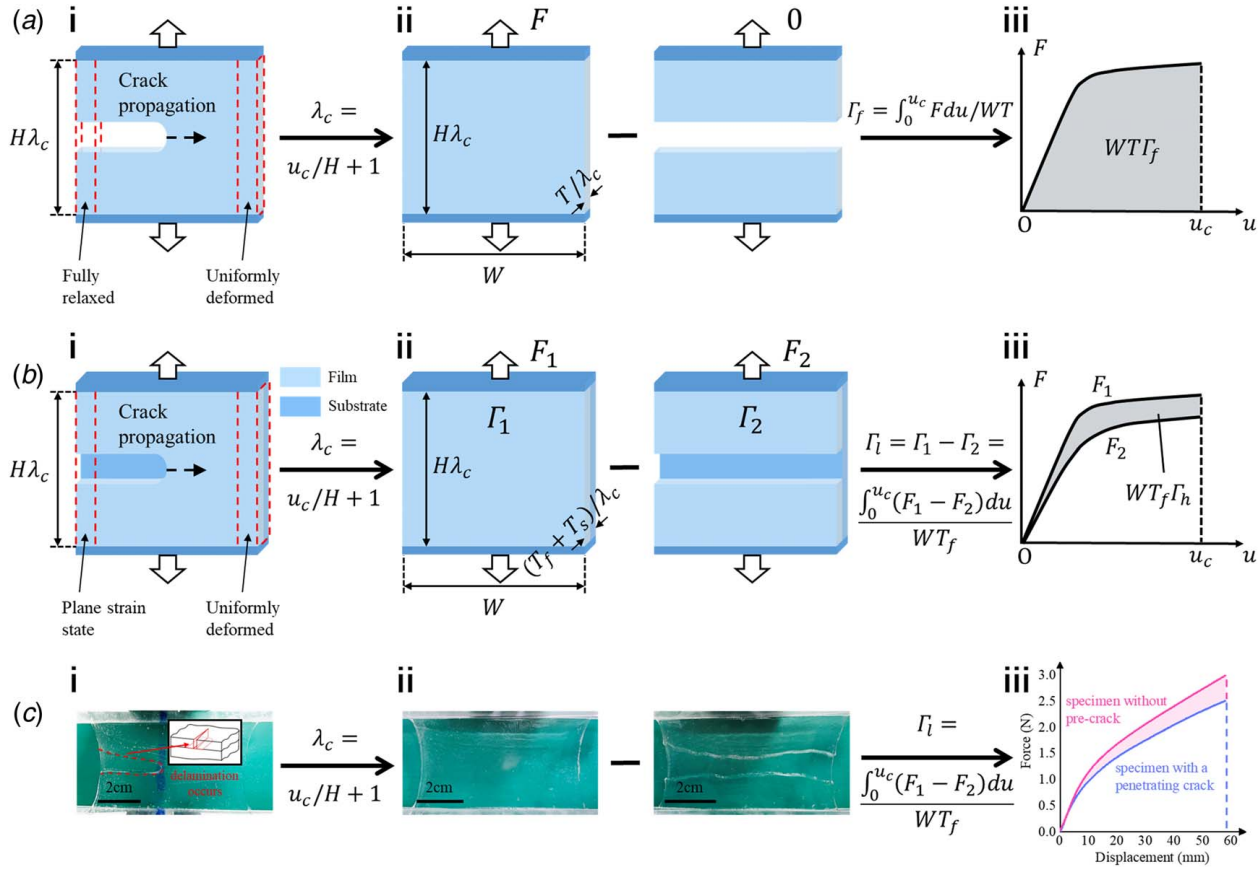

Fig. 1 Pure-shear test on monolayer hydrogels and modified pure-shear test on hydrogel laminates. (*a*) Schematics illustrating the pure-shear test for measuring fracture toughness of monolayer hydrogels: (i) a piece of a hydrogel with a notch was stretched to a critical stretch of λ_c until the crack propagates; (ii) the same piece of hydrogel but without notch was stretched to λ_c with the applied force F recorded; and (iii) the fracture toughness of the hydrogel can be calculated as $\Gamma_f = \left(\int_0^{u_c} F du\right)/WT$. (*b*) Schematics illustrating the modified pure-shear test for measuring fracture toughness of hydrogel laminates: (i) a specimen of hydrogel laminates with a notch was stretched to a critical stretch of λ_c until the crack propagates; (ii) the second specimen without precrack and the third specimen with a penetrating channel crack were stretched to λ_c with the applied force F_1 and F_2 recorded; and (iii) the fracture toughness of the laminates can be calculated as $\Gamma_l = \left[\int_0^{u_c}(F_1 - F_2)du\right]/WT_f$. (c) (i) and (ii) Photos of the modified pure-shear test on the PAAm-PAA hydrogel laminate, and (iii) the corresponding force–displacement curves of the specimens tested.

stretch λ_c recorded. Subsequently, the second specimen without precrack is uniformly pulled to the same stretch of λ_c times of its undeformed length, where the applied force F is noted as a function of the displacement u. Considering that $W \gg H$ in the first specimen, part of the hydrogel far ahead of the crack front or far behind the crack front is either uniformly deformed or fully relaxed, respectively. Hence, the extension of the crack can be treated as a transformation from a uniformly deformed part to a fully relaxed part with the same width, and the energy demanded for the crack to propagate forward a unit area at the undeformed state (i.e., the fracture toughness) can be obtained by the formula $\Gamma_f = \left(\int_0^{u_c} F du\right)/WT$, where F and u have been measured by stretching the second specimen and $u_c = H(\lambda_c - 1)$.

To measure the fracture toughness of the hydrogel laminates composed of two dissimilar materials, it is necessary to modify the experimental setup of the classical pure-shear test considering the laminates' unique characteristics. Unlike testing monolayer hydrogels, three identical specimens of hydrogel laminates are prepared with the same material and geometry sizes, including film thickness T_f, substrate thickness T_s, width W, and height H, where $W \gg H \gg T_f \approx T_s$. As mentioned earlier, the hydrogel laminate's fracture toughness is defined as the energy needed for a crack in the film to advance a unit area. So, a notch with a length of ~0.5 W is introduced into the film of the first specimen (Fig. 1(*bi*)), forming a channel crack. The second specimen (Fig. 1(*b*ii)) is prepared without precrack, and the third specimen's (Fig. 1(*b*iii)) film is slit through, which forms a penetrating channel crack in the width direction. As illustrated in Fig. 1(*b*), all pieces of specimens are clamped along the width direction, and then the first specimen with a precrack of ~0.5 W is gradually pulled in the height direction until the crack starts to propagate in the width direction, with the critical stretch λ_c recorded. Similar to the situation in the pure-shear test on monolayer hydrogels, considering that W is substantially larger than H, the region of the laminate far ahead of the crack front or far behind the crack front is either uniformly deformed or in the plane strain state, respectively, in the first specimen, while the region lying between the uniformly deformed region and the plane strain region is in a complex deformation state due to the crack tip. In this case, an increase in the crack length of amount dc measured in the undeformed state of the specimen does not alter the state of strain in the complex deformed region but just essentially shifts this region along the crack propagation direction by a distance of dc. That is to say, the increase in crack length leads to the plane strain region growing in size by dc at the expense of the uniformly deformed region, accompanied by a change in the specimen's elastic energy. Thus, the energy required for advancing the crack length dc equals the elastic energy stored in a volume of $H(T_f + T_s)dc$ of the specimen in the uniformly deformed region minus the elastic energy stored in a volume of $H(T_f + T_s)dc$ of the specimen in the plane strain region. Thereafter, the second specimen without precrack and the third specimen with a penetrating channel crack are uniformly stretched to the same critical stretch λ_c separately, with the applied force F_1 and F_2 recorded as a function of displacement u. Based on the aforementioned results, the fracture toughness of the hydrogel laminates can be obtained as $\Gamma_l = U/T_f = \left[\int_0^{u_c} (F_1 - F_2) du\right]/WT_f$, where $u_c = H(\lambda_c - 1)$.

2.2 Experimental Results and Analysis. In the actual test, we chose the PAA and PAAm hydrogels as materials for fabricating the hydrogel laminate. The raw materials were purchased from Macklin, Shanghai, China (acrylic acid, AA, A800293; acrylamide, AAm, A800656) and Sigma-Aldrich, Shanghai, China (*N*, *N*′-methylenebis(acrylamide), MBAA, M7279; α-ketoglutaric acid, 75890). To synthesize the hydrogel laminate, we need to synthesize the monolayer PAA hydrogel as the hydrogel film in the first place. Accordingly, we prepare the PAA hydrogel precursor by adding 6.255 g AA into 30 ml de-ionized water, where at the same time, 0.0088 g MBAA (0.024 wt%) and 0.0125 g α-ketoglutaric acid (0.034 wt%) are also mixed into the solution as the cross-linker and the photo-initiator, respectively. Then the precursor is injected into an acrylic mold and subjected to 365 nm ultraviolet radiation (8 W) for 2 h for curing. After cross-linking, the PAA hydrogel is shaped by the mold into a cuboid with the following geometry sizes: 70 mm in width, 30 mm in height, and 1.5 mm in thickness. Next, the substrate of the laminate is fabricated from the PAAm hydrogel as scheduled with similar procedures. To prepare the precursor, we add 6.809 g AAm and 0.0041 g MBAA (0.0072 wt%) as the cross-linker, and 0.0136 g α-ketoglutaric acid (0.024 wt%) as the photo-initiator into 50-ml de-ionized water. Then we inject the precursor into the same mold and put it under UV radiation for an hour for curing. As expected, the mold shapes the PAAm hydrogel into the same geometry size as the hydrogel film, namely, a cuboid of 70 mm × 30 mm × 1.5 mm. To avoid contamination on the surface, freshly synthesized PAA hydrogels and PAAm hydrogels are instantly sticked together with the contact time set to be 30 s. The adhesion is performed at ambient conditions, and there is no applied contact pressure. After the preparation of the hydrogel laminate, a precrack is introduced in the film by a razor blade if necessary. Subsequently, we perform pure-shear tests and modified pure-shear tests on monolayer PAA hydrogel film and PAAm-PAA hydrogel laminates, respectively. The specific methods of the tests have been explained in the previous part. The initial distance between the two clamps is 17 mm, and the stretch rate is set to 2 per minute, and the photos of the experimental process are shown in Fig. 1(*c*).

Also, Fig. 1(*c*) gives the force–displacement curves of the two specimens measured for the modified pure-shear tests. With the information included in these curves, the fracture toughness of the laminate can be calculated according to the method mentioned in Sec. 2.1. Accordingly, Fig. 2 plots this computed toughness of the PAAm-PAA laminate, and the measured toughness of the monolayer PAA hydrogel is also included in the figure as a reference. It can be found that there exists a huge difference between the fracture toughness of the monolayer hydrogel and the laminate, where the latter toughness is almost twice the former. From this perspective, the fracture properties of hydrogel laminates are evidently superior to that of monolayer hydrogels, as it requires much more energy to advance a crack in hydrogel laminates than in hydrogel monolayers, considering that there exists unneglectable energy dissipation during crack propagation. This is due to the film–substrate interfacial delamination's influence on the laminate's toughness, which can be observed in the experiments—as illustrated by the inset of Fig. 1(*c*), when delamination happens, the crack opens widely in the wake of the crack front, with nearly uniform crack opening displacement through the film thickness. Previous studies [24,29–31] have shown that when a multilayer structure consisting

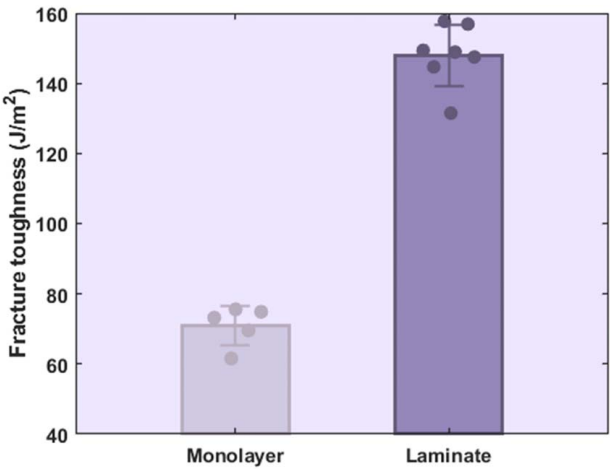

Fig. 2 Fracture toughness of monolayer PAA hydrogels and PAAm-PAA hydrogel laminates measured by pure-shear tests and modified pure-shear tests, respectively

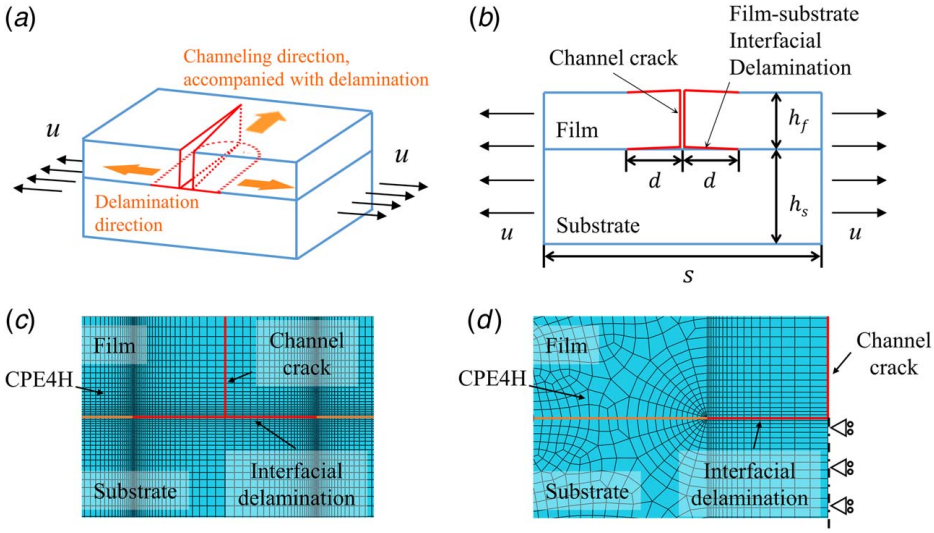

Fig. 3 Computational model for studying the fracture toughness of hydrogel laminates: (*a*) Schematics illustrating steady-state co-evolving channel cracking and interfacial delamination. (*b*) Finite element models for calculating the energy release rate for co-evolving channel cracking and interfacial delamination. Example of finite element mesh for calculating the energy release rate for (*c*) channel cracking and interfacial delamination perpendicular to tensile direction and (*d*) interfacial delamination along tensile direction. In the region near the tip of the interfacial delamination, both the film and the substrate are densely meshed with the CPE4H element.

of brittle film and compliant substrate sustains large deformation, the interfacial delamination is likely to occur subsequently after the channel cracking of the film and then co-evolve with the channel crack, the specific circumstance of which is illustrated in Fig. 3(*a*). This happens because near the channel root of the crack, stress concentration will take place, and when it is severe enough, the interfacial delamination will occur and propagate along the tensile direction. Once the delamination exists, the necessary condition for the crack's advancing in the direction vertical to the applied tension is that it is accompanied by the propagation of interfacial delamination near the root of the crack front, which will create extra demand for energy. Hence, the fracture toughness of the laminates covers the energy required for both the channel crack and the interfacial delamination to propagate. A theoretical and quantitative analysis, along with numerical simulations, of the co-evolving channel cracking and interfacial delamination in hydrogel laminates will be carried out in the next section, aiming to complete the aforementioned explanation for the laminates' enhanced fracture toughness.

3 Theoretical Analysis

Recall that in the previous section, we experimentally measured a PAAm-PAA laminate's fracture toughness using the modified pure-shear test method proposed and found a considerable difference between it and the toughness of monolayer PAA hydrogel. In this section, to further explain this experimentally observed phenomenon, we in detail elaborate on the mechanism of the interfacial delamination co-evolving with the channel cracking during the tests through theoretical analysis and numerical simulations. The expression of the fracture toughness of the hydrogel laminates is proposed and then validated by experimental results.

Concentrating on essentials, we model a hydrogel laminate composed of hydrogel film and substrate under uniaxial tension and analyze the tensile failure of this structure using the finite element code ABAQUS. As illustrated in Fig. 3, when the applied tension is sufficiently large, cracks may initiate from hidden defects in the hydrogel film and then further propagate until a channel crack is formed, inducing serious stress concentration around the channel root, which will then lead to interfacial delamination. As to be shown later, during the propagation of interfacial delamination, its driving force drops as it advances along the direction of tension. As a consequence, the delamination will ultimately stop propagating in the tensile direction when the driving force decreases to a level that is lower than the film–substrate interfacial toughness. For another, the channel crack, accompanied by the interfacial delamination near the root of the crack front, continues to propagate in the direction normal to the applied tension—a process defined as the steady-state co-evolution of channel crack and interfacial delamination.

As a 3D fracture problem, computing the specific stress and deformation state near the front of the channel crack and the accompanied interfacial delamination is costly and sophisticated and, thus, hard to accomplish. In contrast, it is worth noting that the laminate can be regarded as deforming under the plane strain conditions far ahead and far behind the cracking and delamination front. Thus, we simulate a slice of laminate of unit thickness far behind the cracking and delamination front, and the driving force for interfacial delamination in the direction of tension can be obtained by computing the energy release rate at the delaminating front in the same direction, leveraging the J-integral function of ABAQUS. As to the driving force for both the channel cracking and the interfacial delamination to propagate in the direction vertical to the applied tension, taking all materials to be hyperelastic, that can be calculated as the elastic energy stored in a slice of laminate of unit thickness far ahead of the channel front minus the elastic energy stored in a slice of laminate of unit thickness far behind the channel front [32].

In the simulations, the neo-Hookean model is adopted for the hydrogels, and the material parameters are determined by performing uniaxial tensile tests on the PAA and PAAm hydrogels synthesized in the previous experiment and measuring their stress–stretch curves. Here, considering the identical material selection, we reuse the experimental data employed in a previous publication of ours [24] instead of retesting. When $\mu_f = 3$ pKa for PAA film and $\mu_s =$ 2.4 pKa for PAAm substrate, the test data fit well into the neo-Hookean model, supposing that the two hydrogels are both incompressible materials. The geometric dimensions of the hydrogel laminate modeled, namely, the thickness of the hydrogel film h_f, the thickness of the hydrogel substrate h_s, and the length of the laminate

s, are set to be identical to those of the laminates in the previous modified pure-shear tests. Far behind the fracture front, the width of the film–substrate interfacial delamination is d on either side of the channel root. To study its influence on the energy release rate for channel cracking and delamination, we vary the ratio d/h_f, i.e., the normalized delamination width in simulations. In terms of boundary conditions, along the lateral sides of the slice, the horizontal displacement is set to u, which satisfies that the applied stretch $\lambda_{appl} = 2u/s + 1$ is in line with the critical stretch λ_{cr} recorded in preceding modified pure-shear tests on hydrogel laminates. In the region near the tip of the interfacial delamination, both the film and the substrate are densely meshed with the four-node bilinear plane strain quadrilateral, hybrid with constant pressure, concentric-circle elements, i.e., CPE4H element (Fig. 3(*c*)). Aiming to reduce the computation time, we generate the mesh for the rest of the model with bias nodes, where elements near the delamination tip are finer and elements far away from the delamination tip are coarser.

As noted earlier, the total driving force G_{total} for both the channel cracking and the interfacial delamination to propagate in the direction normal to the applied tension (e.g., inset of Fig. 4(*a*)) can be computed as the difference between the elastic energy stored in a slice of laminate of unit thickness far ahead of the fracture front and that far behind the fracture front. Considering the steady-state fracture process, the width of the film–substrate interfacial delamination far behind the crack front will reach a constant d^s. Figure 4(*a*) plots G_{total} as a function of the normalized steady-state delamination width d^s/h_f, and it can be noticed in the figure that G_{total} increases significantly as the steady-state delamination width increases. This can be explained by the vast quantities of elastic energy released from the newly formed delaminated region of the hydrogel film in the propagation of the channel cracking and the concomitant interfacial delamination because of losing substrate constraint. For instance, G_{total} increases almost fivefold when $d^s/h_f = 5$ compared with the case $d^s/h_f = 0.1$. In contrast, without interfacial delamination, only a confined region in the hydrogel film along the channel crack surface is relaxed; thus, the elastic energy released will be modest. Dimensional considerations indicate that the total driving force G_{total} takes a form that

$$G_{total} = q\left(\frac{d^s}{h_f}, \frac{h_s}{h_f}, \frac{\mu_s}{\mu_f}, \lambda_{appl}\right)\mu_f h_f \tag{1}$$

According to Eq. (1), considering that in the simulations the material parameters μ_s and μ_f as well as the geometric parameters h_s and h_f are set to be identical with those of the samples in the experiments, and the applied stretch λ_{appl} is set to the experimentally measured critical stretch, the predicted energy release rate G_{total} only depends on d^s. Thus, based on the experimentally obtained energy release rate for crack propagation valuing 148 J/m^2 (represented by the horizontal dashed lines in Fig. 4(*a*)), the normalized steady-state delamination width d^s/h_f for the samples used in the experiment can be determined as 0.6—by finding the intersection of the dashed line and the calculated energy release rate curve in Fig. 4(*a*).

Next, by computing the energy release rate at the delamination front in the slice far behind the crack front in the direction of tension, we obtain the driving force for interfacial delamination G_d (e.g., inset of Fig. 4(*b*)) and then plot it as a function of normalized delamination width d/h_f in Fig. 4(*b*). In the simulations, taking advantage of the symmetry of the geometry, only half of the hydrogel laminate is modeled, with the symmetric boundary condition set along the symmetry plane (Fig. 3(*d*)). As illustrated in the figure, when the delamination width is small (e.g., $d/h_f < 0.5$), the driving force for interfacial delamination tends to be tremendous as a result of the severe stress concentration around the channel root, but this enormous driving force decreases sharply as the delamination width increases within the range of $d/h_f < 5$. Also, dimensional considerations indicate that the driving force G_d takes a form similar

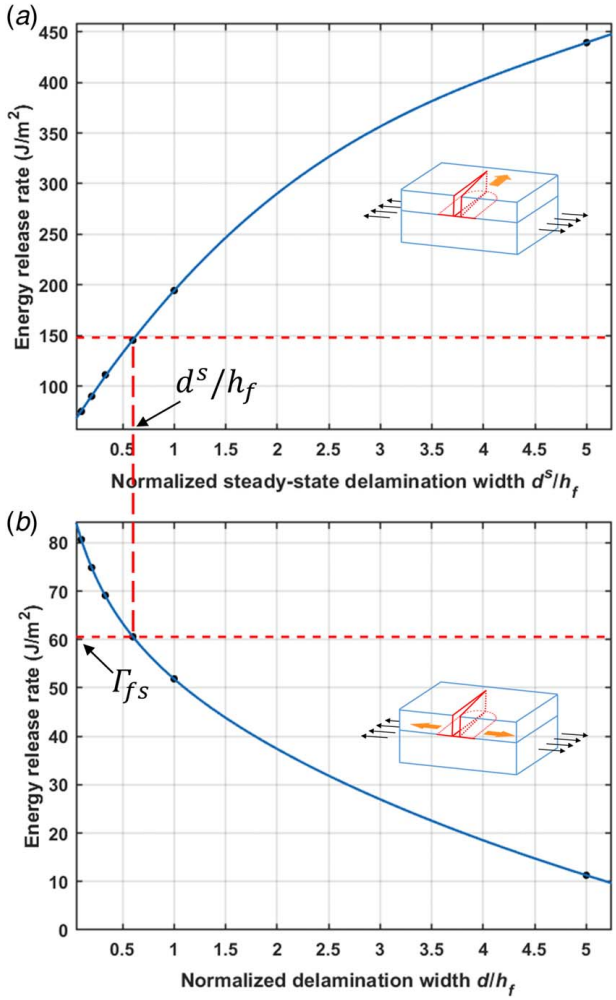

Fig. 4 Simulation results of the co-evolving channel cracking and interfacial delamination. (*a*) Energy release rate for channel cracking and interfacial delamination perpendicular to tensile direction as a function of normalized steady-state delamination width d^s/h_f. Insets: Schematics of the steady-state co-evolving channel cracking and interfacial delamination perpendicular to tensile direction. (*b*) Energy release rate for interfacial delamination along tensile direction as a function of normalized delamination width d/h_f. Insets: The interfacial delamination along tensile direction. Dash lines: Based on the experimentally obtained energy release rate for crack propagation, the normalized steady-state delamination width d^s/h_f for the samples used in the experiment can be determined from (*a*), from which the interfacial toughness Γ_{fs} of the PAAm-PAA interface can be further determined in (*b*).

to Eq. (1) but with a different dimensionless function f that

$$G_d = f\left(\frac{d}{h_f}, \frac{h_s}{h_f}, \frac{\mu_s}{\mu_f}, \lambda_{appl}\right)\mu_f h_f \tag{2}$$

The generation and propagation of the interfacial delamination depend on the comparison between driving force G_d and film–substrate interfacial toughness Γ_{fs} according to the theory of fracture mechanics. It can be observed in Fig. 4(*b*) that delamination may start to form at the channel root when the film–substrate interfacial toughness is modest, and the driving force drops as it advances along the interface between film and substrate in the direction of applied tension. And when the driving force falls to a level in line with the interfacial toughness, i.e., $G_d = \Gamma_{fs}$, propagation of the delamination will ultimately stop, where the final delamination width is d^s. Substituting Eq. (2) into the aforementioned equation, it can be

found that d^s depends on four dimensionless parameters: the thickness ratio h_s/h_f and shear modulus ratio μ_s/μ_f between the substrate and film, the applied stretch λ_{appl}, and the normalized interfacial toughness $\Gamma_{fs}/\mu_f h_f$. Given this, in the simulations, these parameters remain to be identical with those used in the experiments. Then based on Eq. (2) and preceding simulation settings, from the previously obtained steady-state delamination width d^s in the experiment, we can evaluate the interfacial toughness Γ_{fs} of the PAAm-PAA interface as 60.57 J/m^2, which is represented by the horizontal dashed lines in Fig. 4(*b*).

The critical condition for steady-state co-evolving channel cracking and interfacial delamination is given by

$$G_{total} = \Gamma_f + 2\Gamma_{fs} d^s / h_f \tag{3}$$

where Γ_f is the fracture toughness of the hydrogel film, and the last term in the formula denotes the energy necessary for advancing the film–substrate interfacial delamination accompanying the channel crack's per unit area propagation. Substituting the obtained normalized steady-state delamination width d^s/h_f and interfacial toughness Γ_{fs} as well as the experimentally measured fracture toughness of PAA hydrogels $\Gamma_f = 69.9$ J/m^2 (here, we also reuse the testing results in our previous publication [24] for identical material selection) into Eq. (3), the right-hand side of the equation can be calculated as 143 J/m^2, while the left-hand side of the equation, namely, the experimentally obtained energy release rate for crack propagation is 148 J/m^2. It follows then that the equality holds (neglecting experimental and simulation errors)—indicating that our theoretical model is sufficient to explain the experimentally observed phenomenon, and the expression for the fracture toughness of the hydrogel laminates takes the form of $\Gamma_f + 2\Gamma_{fs} d^s/h_f$. That is to say, the film–substrate interfacial delamination is indeed the main cause of the discrepancy in fracture toughness between the PAAm-PAA laminate and the monolayer PAA hydrogel, as the fracture toughness of the laminates covers the energy required for both the crack and concomitant interfacial delamination to propagate in the direction vertical to the applied tension. In addition to boosting the energy needed for cracking in hydrogel laminates, the interfacial delamination can introduce the crack morphology's change and thus relieve the stress concentration near the channel root, while without delamination the substrate will be prone to fracture for being subject to a large stress concentration.

4 Conclusion

In this article, to study the failure mechanism of the vast emerging hydrogel laminates, we conduct an experimental investigation combined with theoretical analysis and numerical simulations focusing on their fracture toughness, which is a less explored but important parameter characterizing the fracture behavior. It is found that the traditional method to measure the fracture toughness of soft materials—performing classical pure-shear tests—has limitations when applied to hydrogel laminates. Thus, a kind of modified pure-shear test suitable for measuring the fracture toughness of hydrogel laminates with a modified experimental setup is proposed, which is then applied to testing a PAAm-PAA laminate's toughness. From the results, it can be found that there exists a striking enhancement in the fracture toughness of PAAm-PAA laminates when compared with the monolayer PAA hydrogel. Through theoretical analysis and numerical modeling, this experimentally observed phenomenon is explained—the fracture toughness of the laminates covers the energy required for both the crack and concomitant interfacial delamination to propagate in the direction vertical to the applied tension, and the theoretical predictions agree well with the experimental results. The results from this study provide quantitative guidance for characterizing the fracture toughness of hydrogel laminates and for in-depth exploration of their failure mechanisms.

Funding Data

- National Key Technologies Research and Development Program (Grant No. 2022YFC3203900).
- Natural Science Foundation of Zhejiang Province (Grant No. LR22A020005).
- National Natural Science Foundation of China (Grant No. 12072314).
- 111 Project (Grant No. B21034).

Conflict of Interest

There are no conflicts of interest.

Data Availability Statement

The authors attest that all data for this study are included in the paper.

References

[1] Wathoni, N., Motoyama, K., Higashi, T., Okajima, M., Kaneko, T., and Arima, H., 2016, "Physically Crosslinked-Sacran Hydrogel Films for Wound Dressing Application," Int. J. Biol. Macromol., **89**, pp. 465–470.

[2] Qazi, T. H., and Burdick, J. A., 2021, "Granular Hydrogels for Endogenous Tissue Repair," Biomater. Biosyst., **1**, p. 100008.

[3] Han, L., Lu, X., Wang, M., Gan, D., Deng, W., Wang, K., Fang, L., et al., 2017, "A Mussel-Inspired Conductive, Self-Adhesive, and Self-Healable Tough Hydrogel as Cell Stimulators and Implantable Bioelectronics," Small, **13**(2), p. 1601916.

[4] Keplinger, C., Sun, J.-Y., Foo, C. C., Rothemund, P., Whitesides, G. M., and Suo, Z., 2013, "Stretchable, Transparent, Ionic Conductors," Science, **341**(6149), pp. 984–987.

[5] Haghiashtiani, G., Habtour, E., Park, S.-H., Gardea, F., and McAlpine, M. C., 2018, "3D Printed Electrically-Driven Soft Actuators," Extreme Mech. Lett., **21**, pp. 1–8.

[6] Sarwar, M. S., Dobashi, Y., Preston, C., Wyss, J. K. M., Mirabbasi, S., and Madden, J. D. W., 2017, "Bend, Stretch, and Touch: Locating a Finger on an Actively Deformed Transparent Sensor Array," Sci. Adv., **3**(3), p. e1602200.

[7] Larson, C., Peele, B., Li, S., Robinson, S., Totaro, M., Beccai, L., Mazzolai, B., and Shepherd, R., 2016, "Highly Stretchable Electroluminescent Skin for Optical Signaling and Tactile Sensing," Science, **351**(6277), pp. 1071–1074.

[8] Lee, Y., Song, W. J., and Sun, J. Y., 2020, "Hydrogel Soft Robotics," Mater. Today Phys., **15**, p. 100258.

[9] Li, X., Yuan, L., Liu, R., He, H., Hao, J., Lu, Y., Wang, Y., Liang, G., Yuan, G., and Guo, Z., 2021, "Engineering Textile Electrode and Bacterial Cellulose Nanofiber Reinforced Hydrogel Electrolyte to Enable High-Performance Flexible All-Solid-State Supercapacitors," Adv. Energy Mater., **11**(12), p. 2003010.

[10] Wu, K. S., Stefik, M. M., Ananthapadmanabhan, K. P., and Dauskardt, R. H., 2006, "Graded Delamination Behavior of Human Stratum Corneum," Biomaterials, **27**(34), pp. 5861–5870.

[11] Qin, M., Sun, M., Bai, R., Mao, Y., Qian, X., Sikka, D., Zhao, Y., Qi, H. J., Suo, Z., and He, X., 2018, "Bioinspired Hydrogel Interferometer for Adaptive Coloration and Chemical Sensing," Adv. Mater., **30**(21), p. 1800468.

[12] Han, Z., Wang, P., Mao, G., Yin, T., Zhong, D., Yiming, B., Hu, X., et al., 2020, "Dual pH-Responsive Hydrogel Actuator for Lipophilic Drug Delivery," ACS Appl. Mater. Interfaces, **12**(10), pp. 12010–12017.

[13] Pan, L., Yu, G., Zhai, D., Lee, H. R., Zhao, W., Liu, N., Wang, H., et al., 2012, "Hierarchical Nanostructured Conducting Polymer Hydrogel With High Electrochemical Activity," Proc. Natl. Acad. Sci. USA, **109**(24), pp. 9287–9292.

[14] Yu, C., Duan, Z., Yuan, P., Li, Y., Su, Y., Zhang, X., Pan, Y., et al., 2013, "Electronically Programmable, Reversible Shape Change in Two- and Three-Dimensional Hydrogel Structures," Adv. Mater., **25**(11), pp. 1541–1546.

[15] Lin, S., Yuk, H., Zhang, T., Parada, G. A., Koo, H., Yu, C., and Zhao, X., 2016, "Stretchable Hydrogel Electronics and Devices," Adv. Mater., **28**(22), pp. 4497–4505.

[16] Sun, J.-Y., Keplinger, C., Whitesides, G. M., and Suo, Z., 2014, "Ionic Skin," Adv. Mater., **26**(45), pp. 7608–7614.

[17] Yang, C. H., Chen, B., Lu, J. J., Yang, J. H., Zhou, J., Chen, Y. M., and Suo, Z., 2015, "Ionic Cable," Extreme Mech Lett., **3**, pp. 59–65.

[18] Jia, Z., Tucker, M. B., and Li, T., 2011, "Failure Mechanics of Organic–Inorganic Multilayer Permeation Barriers in Flexible Electronics," Compos. Sci. Technol., **71**(3), pp. 365–372.

[19] Li, T., Huang, Z. Y., Xi, Z. C., Lacour, S. P., Wagner, S., and Suo, Z., 2005, "Delocalizing Strain in a Thin Metal Film on a Polymer Substrate," Mech. Mater., **37**(2), pp. 261–273.

[20] Cordero, N., Yoon, J., and Suo, Z., 2007, "Channel Cracks in a Hermetic Coating Consisting of Organic and Inorganic Layers," Appl. Phys. Lett., **90**(11), p. 111910.

[21] Lu, N., Suo, Z., and Vlassak, J. J., 2010, "The Effect of Film Thickness on the Failure Strain of Polymer-Supported Metal Films," Acta Mater., **58**(5), pp. 1679–1687.
[22] Lacour, S. P., Chan, D., Wagner, S., Li, T., and Suo, Z., 2006, "Mechanisms of Reversible Stretchability of Thin Metal Films on Elastomeric Substrates," Appl. Phys. Lett., **88**(20), p. 204103.
[23] Shao, X., Cai, Y., Yin, S., Li, T., and Jia, Z., 2022, "Mechanics of Interfacial Delamination in Deep-Sea Soft Robots Under Hydrostatic Pressure," ASME J. Appl. Mech., **90**(2), p. 021009.
[24] Cai, Y., Ma, J., Shen, Z., Shao, X., Jia, Z., and Qu, S., 2023, "Enhancing the Fracture Resistance of Hydrogels by Regulating the Energy Release Rate via Bilayer Designs: Theory and Experiments," J. Mech. Phys. Solids, **170**, p. 105125.
[25] Rivlin, R. S., and Thomas, A. G., 1953, "Rupture of Rubber. I. Characteristic Energy for Tearing," J. Polym Sci., **10**(3), pp. 291–318.
[26] Lake, G. J., and Thomas, A. G., 1967, "The Strength of Highly Elastic Materials," Proc. R. Soc. Lond. Ser. A. Math. Phys. Sci., **300**(1460), pp. 108–119.
[27] Baumberger, T., Caroli, C., and Martina, D., 2006, "Solvent Control of Crack Dynamics in a Reversible Hydrogel," Nat. Mater., **5**(7), pp. 552–555.
[28] Baumberger, T., Caroli, C., and Martina, D., 2006, "Fracture of a Biopolymer gel as a Viscoplastic Disentanglement Process," Eur. Phys J. E Soft Matter, **21**(1), pp. 81–89.
[29] Li, T., and Suo, Z., 2007, "Ductility of Thin Metal Films on Polymer Substrates Modulated by Interfacial Adhesion," Int. J. Solids Struct., **44**(6), pp. 1696–1705.
[30] Lu, N., Wang, X., Suo, Z., and Vlassak, J., 2007, "Metal Films on Polymer Substrates Stretched Beyond 50%," Appl. Phys. Lett., **91**(22), p. 221909.
[31] Lu, N., Wang, X., Suo, Z., and Vlassak, J., 2009, "Failure by Simultaneous Grain Growth, Strain Localization, and Interface Debonding in Metal Films on Polymer Substrates," J. Mater. Res., **24**(2), pp. 379–385.
[32] Hutchinson, J. W., and Suo, Z., 1991, "Mixed Mode Cracking in Layered Materials," *Advances in Applied Mechanics*, J.W. Hutchinson, and T.Y. Wu, eds., Elsevier, New York, pp. 63–191.